Spectroscopic determination of the composition of a 50 kV hydrogen diagnostic neutral beam

X. Feng, M. D. Nornberg, D. Craig, D. J. Den Hartog, and S. P. Oliva

Citation: Review of Scientific Instruments **87**, 11E543 (2016); doi: 10.1063/1.4961269
View online: http://dx.doi.org/10.1063/1.4961269
View Table of Contents: http://scitation.aip.org/content/aip/journal/rsi/87/11?ver=pdfcov
Published by the AIP Publishing

Spectroscopic determination of the composition of a 50 kV hydrogen diagnostic neutral beam

X. Feng,[1] M. D. Nornberg,[1,a)] D. Craig,[2] D. J. Den Hartog,[1] and S. P. Oliva[1]
[1]*Department of Physics, University of Wisconsin–Madison, 1150 University Ave., Madison, Wisconsin 53706, USA*
[2]*Wheaton College, Wheaton, Illinois 60187, USA*

(Presented 8 June 2016; received 3 June 2016; accepted 26 July 2016; published online 6 September 2016)

A grating spectrometer with an electron multiplying charge-coupled device camera is used to diagnose a 50 kV, 5 A, 20 ms hydrogen diagnostic neutral beam. The ion source density is determined from Stark broadened H_β emission and the spectrum of Doppler-shifted H_α emission is used to quantify the fraction of ions at full, half, and one-third beam energy under a variety of operating conditions including fueling gas pressure and arc discharge current. Beam current is optimized at low-density conditions in the ion source while the energy fractions are found to be steady over most operating conditions. *Published by AIP Publishing.* [http://dx.doi.org/10.1063/1.4961269]

I. NEUTRAL BEAM OPTIMIZATION

A 50 kV, 5 A hydrogen diagnostic neutral beam (DNB) with 20 ms pulse provides local measurements of impurity ion emission through charge exchange recombination spectroscopy (CHERS)[1,2] and of core-localized magnetic field through the Motional Stark effect (MSE).[1,2] The DNB is used in low-field RFP discharges in the Madison Symmetric Torus[3] and must provide a sufficiently bright, low divergence source of fast atomic hydrogen that the charge exchange emission from C^{+6} ions is comparable to background emission from electron impact excitation, and the H_α fine structure components are sufficiently resolved in the MSE spectrum. To meet these criteria, we require a beam current of 4 A–5 A and a large fraction of the beam neutrals to be at the primary energy of 50 kV. This energy maximizes the charge exchange cross section with C^{+6} and is sufficiently large to provide enough separation of the Stark components to determine the magnetic field. However, the DNB previously suffered from several deficiencies. The ion source failed to create a discharge reliably, the maximum beam current was reduced to below 4A and was variable during a beam pulse, and the primary energy component varied from 60% to 80%. To correct these problems, the DNB was moved to a test stand which could provide greater availability and diagnostic access. We improved the reliability of the ion source by applying both a −3 kV pulse to an ignition tip near the cathode for 10 μs and a 900 V bias voltage across the cathode and anode for 3 ms to guarantee arc formation. We adjusted the beam by tuning the beam voltage, arc current, fuel line pressure, arc and high voltage module timing, and the magnetic isolation field to maximize the number of ions extracted at the full beam energy with a constant beam current. We introduced better high-voltage standoff in the power supply to achieve 50 kV without breakdown in the air. To verify the impact of these improvements, we measured electron density in the ion source and the fraction of each ion beam species. We determined the dependence of the ion source electron density under various conditions by measuring the Stark broadening of the H_β line[4] and the ions species fractions via the Doppler shifted H_α line.[5–10]

II. SPECTROSCOPIC DIAGNOSIS OF THE NEUTRAL BEAM

Figure 1 shows the experimental setup for the ion source electron density and beam components measurement. The axial view is used to measure the ion source density and the view through a side port is used to measure the Doppler-shift spectrum. The spectrometer (Acton, SpectraPro-2500i) is equipped with an Andor iXon Ultra-897 camera which provides emission measurements with millisecond time resolution and 1800 g/mm grating for a spectral resolution of 0.012 nm/pixel. The full width at half maximum (FWHM) of the instrumental Gaussian broadening of spectrometer near the H_α and H_β lines is 0.017 nm.

To help us understand the plasma conditions which optimize the extracted ion current, we measured the plasma density for a variety of control settings for the ion source. To have optical access to the ion source, we needed to remove the copper beam dump which prevented simultaneous measurement under beam formation conditions. The density is determined from the well-tested approximate formula,[11,12]

$$N_e[m^{-3}] = 10^{23} * (w_s[nm]/4.8)^{1.46808}, \quad (1)$$

where w_s is the FWHM of the Stark broadening of the H_β line. Compared with Stark broadening, the Doppler broadening is negligible and the instrumental broadening is about 15%–20% of the Stark broadening. The Stark broadening is determined from the Lorentzian contribution of a Voigt function fitting with the Gaussian component fixed at the instrumental function. For the ion source electron density measurement, the H_β emission is not spatially localized but originates from the

Note: Contributed paper, published as part of the Proceedings of the 21st Topical Conference on High-Temperature Plasma Diagnostics, Madison, Wisconsin, USA, June 2016.

a)Electronic mail: mdnornberg@wisc.edu.

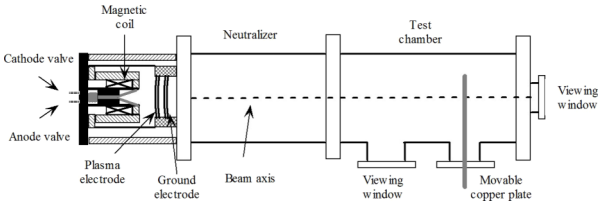

FIG. 1. The DNB is mounted to a vacuum chamber with viewing windows used for spectroscopic measurements of the ion source density and Doppler-shift spectrum of the beam.

entire ion source area; thus, the measured electron density is weighted by the H_β emissivity. We compared these density measurements with beam performance in later beam pulses with the beam dump in place.

For a hydrogen DNB, molecular ions such as H_2^+, H_3^+, and H_2O^+ contribute to the extracted ion current as well as protons. Subsequent collisions in the neutralizer with neutral hydrogen gas will produce a composite beam of H^+ and H^0 with full, half, third, and 1/18 energy via charge transfer and dissociation.[13,14] The fractions of beam particles at each energy are determined by measurement of their Doppler-shifted H_α emission. These fractions are expressed in terms of the line intensities as[6]

$$\frac{H_2^+}{H^+} = C_2[I_{\rm obs}(\frac{E}{2})/I_{\rm obs}(E)],$$
$$\frac{H_3^+}{H^+} = C_3[I_{\rm obs}(\frac{E}{3})/I_{\rm obs}(E)], \quad (2)$$

where I_{obs} is the measured intensity, and C_2 and C_3 are the correction factors obtained by solving a set of ordinary differential equations[13] of beam propagation through the neutral gas using experimental cross section data.[15,16] These order-unity correction factors contain the neutralization efficiency of original beam ions and transition probabilities for spontaneous emission, and depend on the beam voltage and gas density of the neutralizer.

III. EXPERIMENTAL RESULTS AND DISCUSSION

The extracted ion beam current is either limited by space-charge forces or emission. For the space charge limited case, the extracted ion current can be calculated from the Child-Langmuir law: $I_{CL} \propto U^{3/2}/d^2$, where d is the approximate gap width between the electrodes and U is the potential drop. For the emission limited case, the extracted ion current depends on ion source plasma density n_{e0} and temperature T_e as $I_B \propto n_{e0}T_e^{1/2}$. In optimizing the extracted ion current, we found that it increased with grid voltage as expected for space-charge-limited current, but also increased with the arc current in the cathode, and current in the magnetic isolation field coil. These latter two parameters are related to the formation of the plasma at the extraction electrode and their effect on ion current suggests that some type of emission-limited effect plays a role in determining the ion current. We also varied the gas pressure in the gas valves used to fuel the discharge and found that the beam current was reduced at higher pressures. Figure 2 shows the beam current at different fueling pressure and arc current. The error bars depict the beam current variation during the beam pulse. In order to understand the beam behavior, we measured the electron density in the ion source while varying these operational parameters. The measured electron density at different fueling pressure and arc current is shown in Figure 3. The error bars depict the density variation; the fitting error is within 8%. The density ranges from 2.3×10^{20} m^{-3} to 4.5×10^{20} m^{-3} which is consistent in magnitude with the expected operation.[17] It increases with fueling gas pressure, but unexpectedly decreases with arc current. We also find that the density decreases with increased magnetic isolation field strength and the highest constant extracted beam current is achieved for low density conditions. Since we expect greater extracted beam current with n_{e0}, it may be that T_e is changing as well. We would expect T_e to increase with arc current and magnetic isolation field due to greater input power and longer confinement time of the primary electrons. This dependence may also suggest that the shape of the ion sheath at the extraction grid apertures, which is also called the plasma meniscus,[18] is optimized at lower n_{e0}.

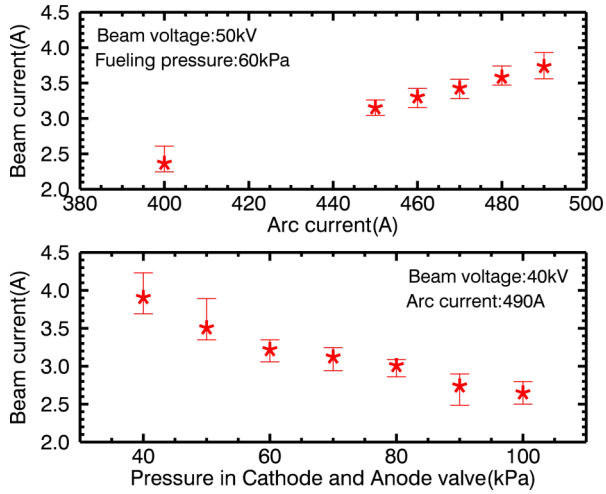

FIG. 2. Beam current at different arc current and different gas pressure in the cathode and anode valve.

We also checked what effect these varying plasma conditions have on the beam energy fractions through measurements of the Doppler-shift spectrum. A typical spectrum of a 50 kV beam observed at 44° to the beam line is shown in Figure 4. The

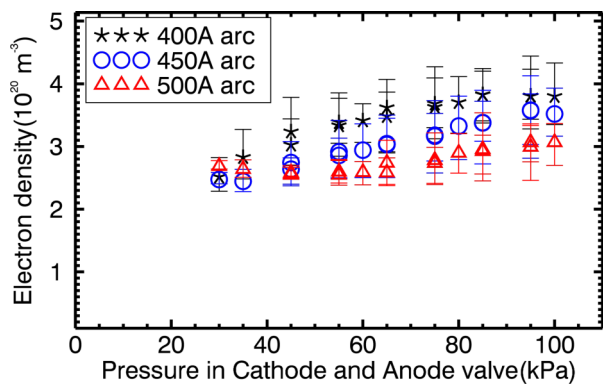

FIG. 3. The electron density of plasma source operating at different gas pressure in the cathode and anode valve and arc current.

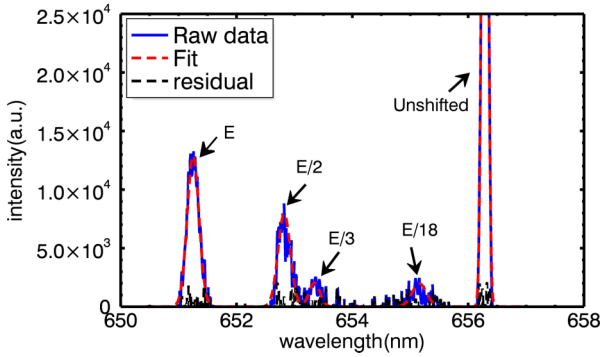

FIG. 4. Spectrum of hydrogen Balmer alpha lines emitted by a 50 kV beam. The four blue shifted lines emitted by beam neutrals and protons originate from H^+, H_2^+, H_3^+, and H_2O^+ in the plasma source.

observation angle is determined by equating the Doppler-shift of the full energy component with the beam energy determined from the grid voltage.

Since the gas line integrated density in the neutralizer and test chamber is estimated at the range of 10^{15} m^{-2}-10^{16} m^{-2}, the C_2 and C_3 at the beam voltage 30 kV–50 kV are estimated to be 0.52–0.4 and 0.36–0.28 with line density of 10^{16} m^{-2}. With these correction factors, the ion species ratios of the beam are estimated from the measured line intensity ratios. The temporal evolution of the original ions species of a 50 kV, 500 A arc current, and 20 ms hydrogen beam is shown in Figure 5. The error bars depict the fitting errors. In addition, the uncertainty in the experimental cross section data[14–16] is 15%. The average ratio of beam ion species with full, half, and one-third energy is 75%:20%:5% and is relatively constant over the beam pulse for different beam voltage, arc current, and fueling gas pressure.

Using the neutralization efficiency[13] of different beam ion species, the ratio of neutrals at full, half, and one-third energy is estimated to be 67%:26%:7%. Compared with prior operation,[19] the fraction of full energy neutrals is enhanced by 7%. Figure 6 shows measurements of the energy fractions before optimization. In comparison with the improved beam, the full energy fraction varies from 60% to 80% during the beam pulse, half energy fraction is much smaller, and one-third energy fraction is larger and also varies over the beam pulse. The evolution of the beam species is determined by the ionization and dissociation processes of hydrogen atoms and

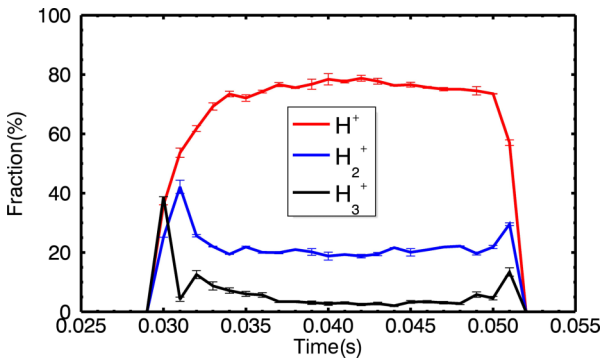

FIG. 5. Temporal evolution of ion species for a 50 kV, 20 ms hydrogen beam.

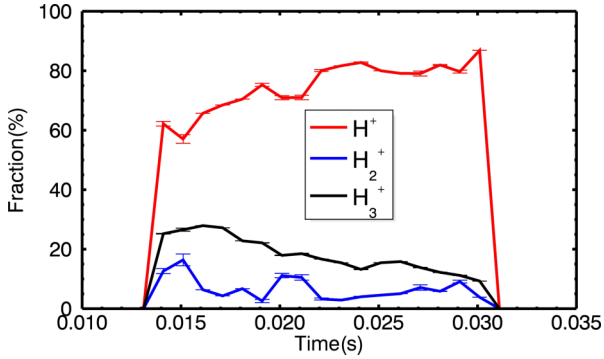

FIG. 6. Temporal evolution of ion species of the DNB before optimization.

molecules in the ion source.[20] The improvement of the beam species and steady beam species ratio in Figure 5 may be due to an increase in T_e. Since H_3^+ is created by H_2^+ collisions with neutral gas and removed by dissociative recombination with electron collisions, the H_3^+ equilibrium population is determined by the relative rate coefficients of these two processes. Considering that H_2^+ is almost constant during the pulse, the dissociation process may be becoming more dominant during the beam pulse, leading to the decrease of H_3^+. The H^+ coming from the dissociation of H_3^+ will contribute to the increase of the total H^+. With the improvements on beam voltage, beam current, and full energy component, the anticipated CHERS signal will increase by 20%–30% and the separation of Stark components will increase by about 10%.

IV. SUMMARY

The DNB has been improved by correcting arcing problems in the power supply and optimizing the extracted ion current by operating the beam at 50 kV, 500 A arc current and 60 kPa–70 kPa fueling gas pressure, creating a steady 4 A beam current with low variation during the beam pulse and full energy ion fraction of 75%. Although the extracted ion current is higher at lower fueling gas pressure, the variation during the beam pulse is the lowest at intermediate gas pressure. Density measurements in the ion source revealed that ion extraction is maximized under low density conditions which are thought to affect the shape of the ion sheath at the extraction grid.

SUPPLEMENTARY MATERIAL

See the supplementary material for figure numerical data.

ACKNOWLEDGMENTS

This work is supported by the U.S. Department of Energy, Office of Science, and Office of Fusion Energy Sciences under Award No. DE-FC02-05ER54814.

[1]D. J. Den Hartog, D. Craig, D. A. Ennis, G. Fiksel, S. Gangadhara, D. J. Holly, and J. C. Reardon, Rev. Sci. Instrum. **77**, 10F122 (2006).
[2]D. Craig, D. J. Den Hartog, G. Fiksel, V. I. Davydenko, and A. A. Ivanov, Rev. Sci. Instrum. **72**, 1008 (2001).
[3]R. N. Dexter, D. W. Kerst, T. W. Lovell, S. C. Prager, and J. C. Sprott, Fusion Sci. Technol. **19**, 131–139 (1991), available at http://plasma.physics.wisc.edu/uploadedfiles/journal/Dexter100.pdf.

[4]H. Griem, *Principles of Plasma Spectroscopy* (Cambridge University Press, 1997).
[5]C. F. Burrell, W. S. Cooper, R. R. Smith, and W. F. Steele, Rev. Sci. Instrum. **51**, 1451 (1980).
[6]R. Uhlemann, R. S. Hemsworth, G. Wang, and H. Euringer, Rev. Sci. Instrum. **64**, 974 (1993).
[7]S. J. Yoo, H. L. Yang, and S. M. Hwang, Rev. Sci. Instrum. **71**, 1421 (2000).
[8]T.-S. Kim, J. Kim, S. R. In, and S. H. Jeong, Rev. Sci. Instrum. **79**, 02A704 (2008).
[9]D. M. Thomas, B. A. Grierson, J. M. Munoz Burgos, and M. A. Van Zeeland, Rev. Sci. Instrum. **83**, 10D518 (2012).
[10]P. Bharathi and V. Prahlad, J. Appl. Phys. **107**, 123307 (2010).
[11]N. Konjevic, M. Ivkovic, and N. Sakan, Spectrochim. Acta, Part B **76**, 16 (2012).
[12]M. A. Gigosos, M. A. Gonzalez, and V. Cardenoso, Spectrochim. Acta, Part B **58**, 1489 (2003).
[13]J. Kim and H. H. Haselton, J. Appl. Phys. **50**, 3802 (1979).
[14]K. H. Berkner, R. V. Pyle, and J. W. Stearns, Nucl. Fusion **15**, 249 (1975).
[15]I. D. Williams, J. Geddes, and H. B. Gilbody, J. Phys. B **15**, 1377 (1982).
[16]I. D. Williams, J. Geddes, and H. B. Gilbody, J. Phys. B **16**, L765 (1983).
[17]A. A. Ivanov, V. I. Davydenko, P. P. Deichuli, G. I. Shulzhenko, and N. V. Stupishin, Rev. Sci. Instrum. **79**, 02C103 (2008).
[18]I. G. Brown, *The Physics and Technology of Ion Sources*, 2nd ed. (Wiley-VCH, New York, 2004).
[19]S. T. A. Kumar, D. J. Den Hartog, B. E. Chapman, M. O'Mullane, M. Nornberg, D. Craig, S. Eilerman, G. Fiksel, E. Parke, and J. Reusch, Plasma Phys. Controlled Fusion **54**, 012002 (2012).
[20]C. F. Chan, C. F. Burrell, and W. S. Cooper, J. Appl. Phys. **54**, 6119 (1983).